

# PCCP

Accepted Manuscript



This article can be cited before page numbers have been issued, to do this please use: A. Kathiravan, S. Venkatesan, P. Murugesan, J. Madhavan, P. Nagaraj and S. Anandan, *Phys. Chem. Chem. Phys.*, 2015, DOI: 10.1039/C5CP05338B.



This is an *Accepted Manuscript*, which has been through the Royal Society of Chemistry peer review process and has been accepted for publication.

*Accepted Manuscripts* are published online shortly after acceptance, before technical editing, formatting and proof reading. Using this free service, authors can make their results available to the community, in citable form, before we publish the edited article. We will replace this *Accepted Manuscript* with the edited and formatted *Advance Article* as soon as it is available.

You can find more information about *Accepted Manuscripts* in the [Information for Authors](#).

Please note that technical editing may introduce minor changes to the text and/or graphics, which may alter content. The journal's standard [Terms & Conditions](#) and the [Ethical guidelines](#) still apply. In no event shall the Royal Society of Chemistry be held responsible for any errors or omissions in this *Accepted Manuscript* or any consequences arising from the use of any information it contains.

Cite this: DOI: 10.1039/c0xx00000x

www.rsc.org/xxxxxx

## ARTICLE TYPE

# A Diminutive Modification in Arylamine Electron Donors: Synthesis, Photophysics and Solvatochromic Analysis – Towards the Understanding of Dye Sensitized Solar Cell Performances

Venkatesan Srinivasan,<sup>1</sup> Murugesan Panneer,<sup>2</sup> Madhavan Jaccob,<sup>2</sup> Nagaraj Pavithra,<sup>3</sup> Sambandam Anandan,<sup>3</sup> Arunkumar Kathiravan<sup>1\*</sup>

Received (in XXX, XXX) Xth XXXXXXXXX 20XX, Accepted Xth XXXXXXXXX 20XX

DOI: 10.1039/b000000x

Electron rich donor moiety plays an important role in dye sensitized solar cells (DSCs). In order to attain a suitable donor moiety for DSCs, deeper understanding of the role of donor moiety in the dye excited state is significant. In this context, arylamine dyes based different electron donor moieties (TRA, CRA and PyRA) were successfully synthesized and well characterized by using <sup>1</sup>H, <sup>13</sup>C-NMR and EI-MS spectrometry. Their photophysical properties and solvatochromic behavior were studied by using UV-Visible absorption, steady state and time resolved fluorescence spectroscopic techniques. The absorption of arylamine dyes is due to intramolecular charge transfer (ICT) between the donor and rhodanine-3-acetic acid via  $\pi$ -bridge, which is further confirmed by DFT calculations. Lippert-Mataga analysis on the solvatochromic data implies that these molecules are more polar in the excited state, which is additional support for ICT. Further, nanocrystalline TiO<sub>2</sub>-based dye-sensitized solar cells (DSCs) were fabricated using these dyes to investigate the influence of donor moieties on their photovoltaic performance. The overall power conversion efficiencies of 2.57%, 1.68% and 1.25% were obtained for TRA, PyRA and CRA dyes, respectively. The enhanced power conversion efficiency of TRA is due to longer lifetime of injected electrons as demonstrated by the electrochemical impedance spectroscopy (EIS) measurements.

## Introduction

Dye-sensitized solar cells (DSCs) is a promising low-cost alternative to traditional silicon-based photovoltaic cells.<sup>1</sup> As a key component of DSCs, sensitizer play a crucial role in light harvesting and light-to-electricity conversion; extensive effort has, therefore, several ruthenium, porphyrin, and organic dyes have been synthesized and investigated in terms of their performance in DSCs.<sup>2-6</sup> Ruthenium dyes offer an average efficiency of 11%, but their application might be limited due to the scarcity of ruthenium metal and environmental concerns.<sup>7-9</sup> Porphyrins are among the most widely studied sensitizers due to their intense absorption in Soret and Q bands to harvest solar energy efficiently in a broad spectral region.<sup>10-18</sup> More importantly, their optical, photophysical, and electrochemical properties can be modulated with peripheral modifications or inner metal coordinations.<sup>19-22</sup> Several porphyrin monomers have been used in DSCs and record high efficiencies of 12% and 13% were achieved by GY50 and SM315 porphyrin dyes, respectively, using a cobalt electrolyte under standard one-sun illumination.<sup>23,24</sup>

Besides, more efforts have been devoted to the development of metal-free organic sensitizers in recent years for the wide availability of the raw materials.<sup>25</sup> Particularly, organic dyes with D- $\pi$ -A configuration are popular for their non-toxicity, high molar extinction coefficients, flexible molecular engineering, and material abundance. Various organic molecules,<sup>26</sup> such as

merocyanine, coumarin, indoline, squaraine, hemicyanine, phenothiazine, triphenylamine, fluorene, carbazole and tetrahydroquinoline have been reported and thus making organic dyes profitable in their application to DSCs. In 2010, Wang et al. have demonstrated the substituted arylamine dye with  $\eta$  up to 10.3% for a metal-free organic dye with an iodine/iodide redox shuttle.<sup>27</sup> Later in 2011, Grätzel et al. reported the phenyldihexyloxy-substituted TPA (DHO-TPA) dye, which exhibited a power conversion efficiency ( $\eta$ ) of 10.3% in combination with a cobalt redox shuttle.<sup>28</sup> In 2013, Wang et al. tailored a metal-free organic dye with the chromophoric core of cyclopentadithiophene-benzothiadiazole (CPDT-BT), which displays power conversion efficiencies at various irradiances of the simulated air mass (AM) 1.5 sunlight of 11.5–12.8%, setting a new benchmark for organic dye-sensitized solar cells.<sup>29</sup> This is the highest conversion efficiency of metal free organic dyes reported so far. Therefore, arylamine dyes have been found desirable candidates for organic sensitizers.

We are particularly interested in the design and synthesis of arylamine dyes to study the role of donor moiety on the excited state properties. In fact, minor changes in the structure of arylamine donors can lead to notable enhancement in the performance of the dye, and its thermal and photochemical stability. For instance, Chen and co-workers reported a family of triphenylamine dyes with an increased electron density of donor moiety as an effective way to improve the dye performance.<sup>30</sup> Dye (TPAR4) with a CH<sub>2</sub>=CH- substituted triphenylamine

electron donating group gave 5.8% efficiency under AM 1.5 G irradiation due to the increase of the electron density in the donor subunit. The corresponding dye (TPAR1)<sup>30</sup> without the CH<sub>2</sub>=CH- substitution exhibited a lower efficiency of 4.3%.

Hagberg et al. developed a very simple modification of arylamine dyes namely D7 and D11 sensitizers.<sup>31</sup> The overall conversion efficiency of D7 and D11 are 5.43% and 7.03% respectively. The higher efficiency of D11 sensitizer compared to D7 sensitizer demonstrates the beneficial influence of alkoxy units on photovoltage and photocurrent, caused by the enhanced red response. The increased photovoltage of D11-sensitized solar cell compared to that of the D7-sensitized solar cell is mainly due to the increased lifetime of the conduction-band electrons.

Here, our aim is to develop the arylamine derivatives with very simple modification and to investigate the role of donor moieties on excited state properties and to correlate the solar cell performance. In the arylamine dyes, taking TRA (diphenylamine donor) as a prototype, CRA and PyRA dyes were developed. In TRA, the free phenyl groups are closed in order to obtain rigid carbazole donor (CRA), whereas, to form pyrrolidino donor (PyRA) two phenyl groups were detached from the carbazole structure (Figure 1). To the best of our knowledge, there are no systematic studies carried out on these molecules. Steady state and time resolved spectroscopic analysis were performed to understand the influence of donor moieties.

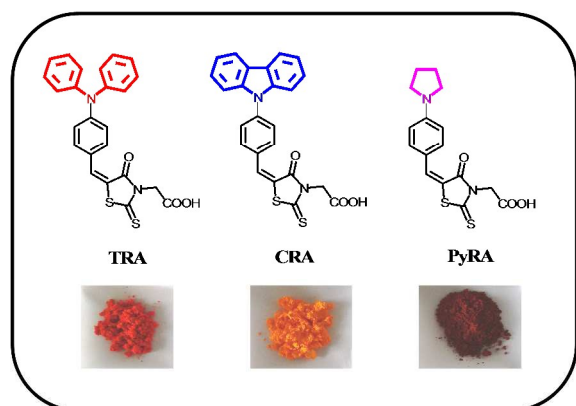


Figure 1: Molecular Structure and photograph of TRA, CRA, PyRA dyes

## Experimental section

### Materials

Rhodanine-3-acetic acid, 4-(diphenylamino)benzaldehyde, N-(4-formylphenyl)carbazole, 4-(1-pyrrolidino)benzaldehyde, and dimethyl sulfoxide-*d*<sub>6</sub> (DMSO-*d*<sub>6</sub>) were purchased from Sigma-Aldrich. Glacial acetic acid and ammonium acetate were purchased from Sisco Research Laboratories (SRL), India and were used without further purification unless otherwise noted. The solvents used for photophysical studies were HPLC grade.

### Instrumentation

Infrared spectrometer (IR) spectra were recorded on BRUKER VERTEX 70 Attenuated total reflection-Fourier transform

infrared spectroscopy (ATR-FTIR) spectrometer. Nuclear magnetic resonance (NMR) spectroscopy was performed on a BRUKER spectrometer operating at 400 MHz for <sup>1</sup>H and 100 MHz for <sup>13</sup>C and collected at ambient probe temperature with spectra calibrated to either internal tetramethylsilane (TMS) standard or to a residual protio solvent. Electron ionization-Mass spectra (EI-MS) analyses were acquired using JEOL GC mate-II mass spectrometer photomultiplier tube (PMT) detector. Cyclic voltammetry (CV) and differential pulse voltammetry (DPV) were recorded using a CHI-620B Electrochemical Analyzer, CH Instruments Inc. A three-electrode single-compartment cell with a glassy carbon working electrode, a platinum wire counter electrode, and Ag/AgCl reference electrode were employed for the experiments. The glassy carbon electrode was polished with Al<sub>2</sub>O<sub>3</sub> paste, cleaned thoroughly in an ultrasonic water bath, and washed with ethanol before each measurement. In the present study, the oxidation potential of arylamine dyes was measured in acetonitrile (ACN) with tetrabutylammonium hexafluorophosphate (0.1 M) as electrolyte. About 10 ml of 1 × 10<sup>-3</sup> M arylamine dyes in acetonitrile is charged with tetrabutyl ammonium hexafluorophosphate was taken in an electrochemical cell and degassed by bubbling nitrogen for 15 min before the experiments. The electronic absorption spectra of samples were recorded using CARY 100 Bio UV-visible spectrophotometer.

The fluorescence spectral measurements were carried out using Fluoromax-4 spectrofluorometer (Horiba Jobin Yvon). For fluorescence studies, much diluted solutions were used to avoid spectral distortions due to the inner-filter effect and emission reabsorption. Time resolved picosecond fluorescence decays were obtained by the time-correlated single-photon counting (TCSPC) technique with microchannel plate photomultiplier tube (Hamamatsu, R3809U) as detector and femtosecond laser as an excitation source. The second harmonics (400 nm) output from the mode-locked femtosecond laser (Tsunami, Spectra physics) was used as the excitation source. The instrument response function for TCSPC system is ~50 ps. The data analysis was carried out by the software provided by IBH (DAS-6), which is based on deconvolution technique using nonlinear least-squares methods. Femtosecond fluorescence decays have been collected using fluorescence up-conversion technique. In our femtosecond up-conversion setup (FOG 100, CDP, Russia) the sample was excited using the second harmonic (400 nm) of a mode-locked Ti-sapphire laser (Tsunami, Spectra physics). The fundamental beam (800 nm) was frequency doubled in nonlinear crystal (1 mm BBO, θ = 25°, φ = 90°) and used for the excitation. The sample was placed inside a 1 mm-thick rotating quartz cell. The fluorescence emitted from the sample was up-converted in a nonlinear crystal (0.5 mm BBO, θ = 38°, φ = 90°) using the fundamental beam as a gate pulse. The upconverted light is dispersed in a monochromator and detected using photon counting electronics. The instrument response function of the apparatus is 300 fs. The femtosecond fluorescence decays were fitted using a Gaussian shape for the excitation pulse.

### DFT calculations

The geometry optimization and harmonic vibrational frequency calculations of the TRA, CRA, PyRA dyes were carried with the

Gaussian09 program package.<sup>32</sup> The ground state geometries of three dyes were optimized by using the DFT method and the hybrid B3LYP<sup>33-35</sup> functional and the 6-311+G\*\* basis set on all atoms. The vibrational analysis was performed at each stationary point found, that confirm its identity as an energy minimum on the potential energy surface and there is no imaginary frequency. The choice of the B3LYP functional was based on previous theoretical studies that show that B3LYP is very successful in the prediction of photophysical properties of this class of compounds.<sup>36</sup>

### Quantum yield measurements

Fluorescence quantum yield ( $\phi_F$ ) of arylamine derivatives were calculated by using following equation (1)

$$\phi_F = (A_R/A_S) (I_S/I_R) (\eta_S/\eta_R)^2 \phi_R \quad \rightarrow (1)$$

where, the subscripts S and R refers to the samples and the reference, respectively.  $A$  is the absorbance at the excitation wavelength,  $I$  is the integrated emission area, and  $\eta$  is the solvent refraction index. Coumarin-153 ( $\phi=0.58$ )<sup>37</sup> used as a standard for CRA and fluorescein ( $\phi=0.9$ )<sup>38</sup> was used as a standard for TRA and PyRA.

### Cell assembly and characterization

FTO glass plates were purchased from BHEL, INDIA. The photoanode<sup>39</sup> was prepared by the following procedure: 0.5 g of TiO<sub>2</sub> (P25) nanoparticles and 0.016 g of polyethylene glycol were added to a solution of 1 M HNO<sub>3</sub>. Then, 0.21 ml of acetyl acetone and 0.04 ml of Triton-X was added to the mixture. Later the mixture was ultrasonicated for 1 h then stirred for 24 h to get homogenous TiO<sub>2</sub> paste. Before the preparation of electrodes, FTO plates were washed by sonicating subsequently in a soap solution, distilled water, acetone, and 2-propanol for 15 min. For photoanode preparation, the washed FTO plates were pretreated with 40 mM solution of TiCl<sub>4</sub> for 30 min at 70 °C. After TiCl<sub>4</sub> treatment, the plates were washed with water and ethanol and then dried at 100 °C on a hot plate for 10 min. Then, the TiO<sub>2</sub> paste was coated on FTO plate by doctor blade technique. Then, the plates were sintered at 450 °C for 30 min to remove the binder, solvent and getting an electrically-connected network of TiO<sub>2</sub> particles by sintering under tubular furnace. After the sintering process, when the temperature of the plate drops to 80 °C, it was immersed into the dye solution in methanol for 24 h. Excess non-adsorbed dye were washed with anhydrous ethanol. The platinum catalyst counter electrode was prepared by deposition of H<sub>2</sub>PtCl<sub>6</sub>.6H<sub>2</sub>O solution (0.005 M in isopropanol) onto FTO glass and then sintering at 450 °C for 30 min. The DSC device was fabricated by the following method: the Pt cathode was placed on top of the photoanode and was tightly clipped together. Then, liquid electrolyte 0.05 M I<sub>2</sub>/0.5 M LiI/0.5 M 4-tertbutyl pyridine (TBP) in 3-methoxypropionitrile was injected in between the two electrodes. The thickness of the electrolyte layer is maintained about 50 μm (approximately thickness of a tape). Photocurrent–voltage characteristics and electrochemical impedance spectra (EIS) of the DSCs were done under 85 mW

cm<sup>-2</sup> light illuminations by using an AUTOLAB12/FRA2 electrochemical analyzer.

## Result and Discussion

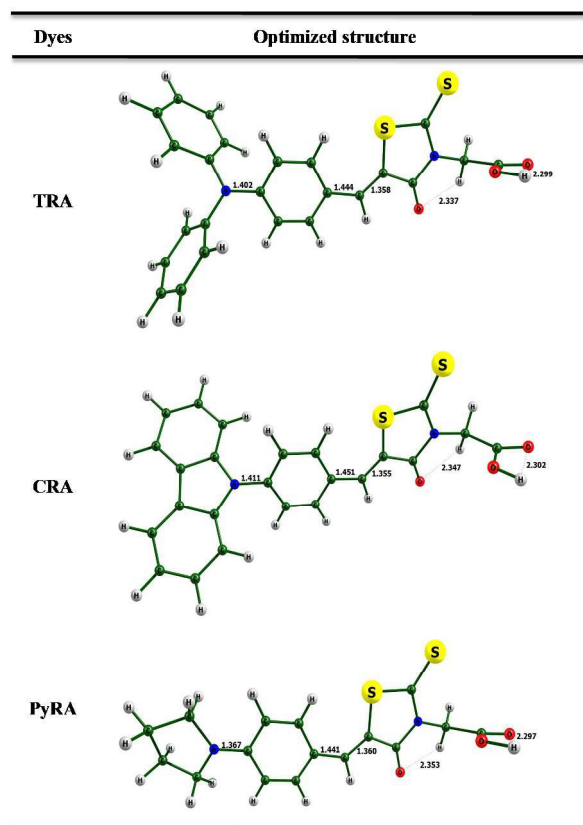
### Molecular design and synthesis

The electron donor moiety in organic sensitizers plays a crucial role in determining the overall power conversion efficiency.<sup>40-42</sup> Therefore, we have targeted three different donor moieties containing arylamine dyes to investigate the role of electron donor moiety on the HOMO-LUMO energy gap, electrochemical, photophysical and photovoltaic properties. Note that, in the targeted dyes,  $\pi$ -bridge (benzene) and acceptor/anchoring group (rhodanine-3-acetic acid) were remained same. The targeted dyes (TRA, CRA and PyRA) were obtained via Knoevenagel condensation of the corresponding aldehydes with rhodanine-3-acetic acid in presence of acetic acid and ammonium acetate. The aldehydes used were 4-(diphenylamino) benzaldehyde, N-(4-formylphenyl)carbazole and 4-(1-pyrrolidino)benzaldehyde. The final products were obtained in good yields and successfully characterized by FT-IR, NMR and mass spectroscopic techniques. The detailed synthetic route (Scheme S1) and characterization data were illustrated in the supporting information (Figure S1-S9). In the arylamine dyes, taking TRA (diphenylamine donor) as a prototype, CRA and PyRA dyes were developed. In TRA, the free phenyl groups are closed in order to obtain rigid carbazole donor (CRA), whereas, to form pyrrolidin donor (PyRA) two phenyl groups were detached from the carbazole structure. Structures and photograph of the synthesized arylamine dyes are depicted in figure 1, which clearly reveals that upon changing the donor moieties, colour of the dyes are remarkably intensified, which is due to the reduced HOMO-LUMO band gaps.

### Theoretical consideration

Density functional theory calculations were employed to investigate the impact of donor moiety on the structure and HOMO/LUMO levels of arylamine dyes. Optimized geometries of TRA, CRA and PyRA along with notable structural parameters are shown in figure 2a, which clearly reveals that intramolecular hydrogen bonding interactions facilitates the most stable conformation of arylamine dyes under investigation. The N<sub>pyr</sub>-C<sub>phenyl</sub> bond length in PyRA (1.367 Å) is shorter than the TRA (1.402 Å) and CRA (1.411 Å). But in the case of TRA and CRA, N<sub>pyr</sub>-C<sub>phenyl</sub> bond distance is closer to single bond length of 1.47 Å. This leads to decrease the effective delocalization in CRA and TRA. This suggest that PyRA dye molecule attributed with partial double bond character, which leads to effective delocalization through out the molecule than the other two dye molecules. In addition to this, PyRA is found to have planar structure whereas in TRA and CRA dyes, the donor moiety is lying perpendicular to the acceptor and  $\pi$  bridge moieties, as a result effective charge transfer is expected to be more in PyRA than TRA and CRA. Upon investigating the ground state dipolemoment of three dye molecules, PyRA has relatively larger dipole moment of 11.08 D compared to the others, TRA (8.55 D)

and CRA (4.53 D). This is the additional support of PyRA is said to have effective intramolecular charge separation between the donor and acceptor units.



5 **Figure 2a:** Optimized geometries of the dyes.

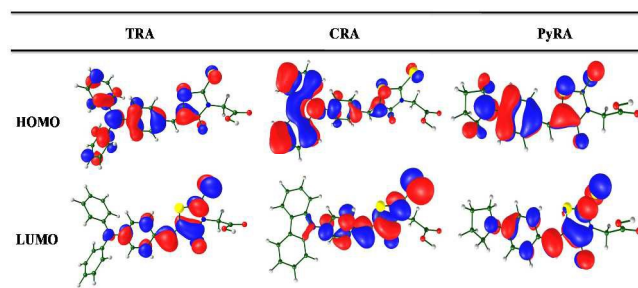


**Figure 2b:** HOMO and LUMO levels of the dyes.

It is very important to analyze the nature of HOMO and LUMO levels of organic dyes prior to study their photovoltaic properties.

The ground state density plots of the HOMO and LUMO of three dye molecules calculated at the B3LYP/6-311+G(d,p) level of theory in THF medium are shown in **figure 2b**. The HOMO is mainly delocalized over the donor unit and the LUMO is originated on the acceptor and spacer units. Hence, the HOMO-LUMO excitation by light irradiation induced the shift of electron from donor moiety to the acceptor moiety via  $\pi$ -bridge. This indicates that the HOMO-LUMO transitions bear a significant intramolecular charge transfer (ICT) character. Notably, the contribution of HOMO levels are higher in donor part of the TRA and CRA. But, in the case of PyRA, the contribution of HOMO level are localized in the entire molecule. Moreover, in all the dyes, the LUMO levels are largely localized in the acceptor part

(rhodanine-3-acetic acid), this is an essential prerequisite for charge transfer properties to the conduction band of TiO<sub>2</sub>. Furthermore, the LUMO is mainly concentrated on the carbonyl and thiocarbonyl group of rhodanine framework and not extending further to the carboxyl group. Hence, charge transfer cannot be transfer through carboxylate group, consequently through space charge transfer likely for the selected dyes.

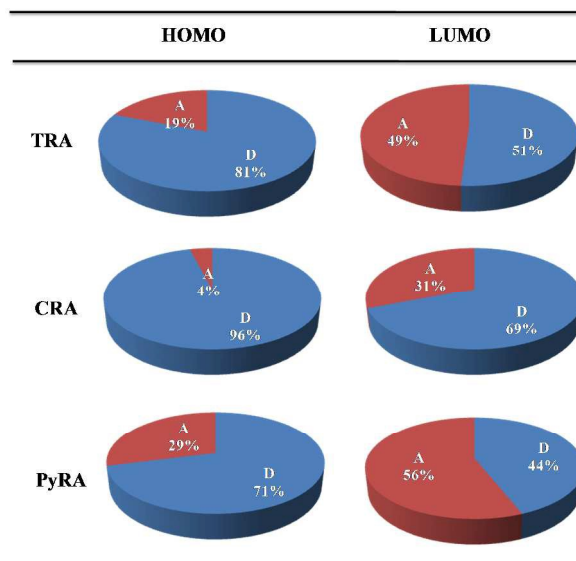


**Figure 3.** Molecular orbital composition (%) in the ground state for dye molecules

It is noteworthy to analyze and understand the origin of individual contributions of various segments of the dye molecules towards HOMO and LUMO levels. So, Chemission program was used to compute the individual contributions of various fragments of the dyes. The entire molecule was fragmented into two groups, namely donor and acceptor groups **figure 3**. Major contributions of HOMO in all the dyes are spread on the donor moiety and it is greater in CRA (96%), TRA (81%) and lower in PyRA (71%) whereas the delocalization of LUMO electron density on acceptor unit of PyRA (69%) is higher than the other two dye molecules (44% and 31% for TRA and CRA respectively). It clearly indicates that the pyrrolidin unit in PyRA facilitates the effective charge transfer from donor to acceptor. Overall, theory results enlightens that, PyRA is found to have excellent charge transfer properties and hence this molecule may show better solar cell power conversion efficiency than other dyes.

#### Steady-state absorption spectroscopy

To obtain a highly efficient DSC, the light harvesting efficiency of dye in photoanode is the most important and indispensable factor, which is mainly related to the molar extinction coefficient of the dye.<sup>43</sup> Therefore, we intend to measure the molar extinction coefficient of arylamine dyes by using UV-visible absorption spectrophotometer. In addition, by measuring absorption spectra of arylamine dyes (TRA, CRA and PyRA), one can understand the influence of electron donors on the light harvesting properties. Hence, UV-vis absorption spectra of the arylamine dyes were recorded in methanol, shown in **figure 4a**.

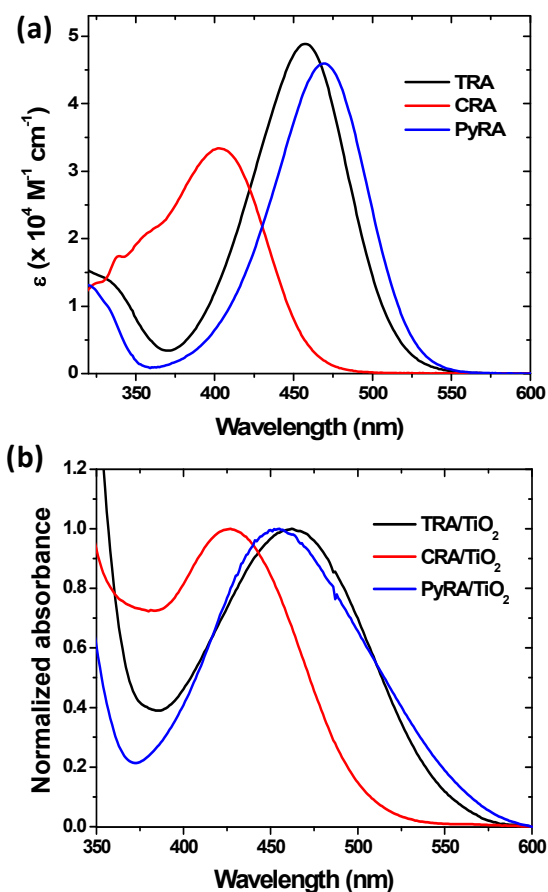


Figure 4: Absorption spectra of TRA, CRA and PyRA (a) in MeOH (b) on TiO<sub>2</sub> film

The absorption of arylamine dyes are due to intramolecular charge transfer (ICT) between the donor to the rhodanine-3-acetic acid via  $\pi$ -bridge. As the concentration of arylamine dyes were increased, the absorbance of the band regularly increased and at the same time, Beer–Lambert’s law was obeyed for all the dyes in the concentration range of  $0.5 \times 10^{-5}$  M to  $2.5 \times 10^{-5}$  M. The maximum absorption peaks and the corresponding molar extinction coefficient values of the dyes were 456 nm ( $4.8 \times 10^4$  M<sup>-1</sup>cm<sup>-1</sup>) for TRA, 403 nm ( $3.3 \times 10^4$  M<sup>-1</sup>cm<sup>-1</sup>) for CRA, and 466 nm ( $4.6 \times 10^4$  M<sup>-1</sup>cm<sup>-1</sup>) for PyRA, respectively. In comparison with the conventional ruthenium dye N719 ( $1.47 \times 10^4$  M<sup>-1</sup>cm<sup>-1</sup> at 535 nm),<sup>44</sup> the arylamine dye molecules showed obviously higher absorption coefficients, which could be beneficial for better light harvesting. By comparing all the dyes, PyRA absorbs at longer wavelength with high molar absorption coefficient, due to strong electron donating ability of pyrrolidin unit to the acceptor via benzene  $\pi$ -bridge. On the other hand, TRA molecule show a hypsochromic shift (10 nm) while compared with PyRA, which is due to electrons are delocalized in the phenyl rings and hence electron-push effect was slightly diminished. However for CRA, a large hypsochromic shift was observed by compared with PyRA, due to the planar nature of carbazole donor favours the delocalization of the lone pair electron of the nitrogen atom, which leads to the decrease in the electron-push effect.<sup>45</sup> Further investigation, absorption spectra of the arylamine dyes were measured in various solvents and

shown in **figure S10-S12**. As seen from the figure, the absorption maximum of the dye is not much shifted with increasing solvent polarity, which implies that the effect of solvent in the ground state is not significant.

In order to understand the light harvesting properties of arylamine dyes on TiO<sub>2</sub> surface, 4  $\mu$ m-TiO<sub>2</sub> nanocrystalline films were prepared from a commercially available TiO<sub>2</sub> paste (Solaronix SA, Ti-Nanoxide HT/SC series) and they were sensitized in a 0.5 mM of arylamine dyes in methanol at room temperature for 1h. The normalized UV-vis absorption spectra of arylamine dyes deposited on transparent TiO<sub>2</sub> films are shown in **figure 4b**. The maximal absorption peaks for TRA, CRA and PyRA on TiO<sub>2</sub> films appeared at 465, 425 and 455 nm, respectively. Moreover, their absorption spectra on TiO<sub>2</sub> film are broadened due to the interaction of the anchoring group of the dyes with TiO<sub>2</sub> which was commonly observed for dye/TiO<sub>2</sub> systems.<sup>46,47</sup> This spectral broadening allows the dye molecules to harvest visible light more efficiently and thus increases the photocurrent response region with a rise of short-circuit current density ( $J_{SC}$ ).<sup>48,49</sup> Except PyRA, compared to the spectrum of TRA and CRA in methanol solution, a red shift of the absorption peak was observed on TiO<sub>2</sub> surface, which can be attributed to the formation of J-aggregate. Interestingly, PyRA/TiO<sub>2</sub> exhibits a blue (at peak maximum) and red (at peak tail) shift while compared with its spectrum in methanol solution, thus indicating the mixture of H and J-type aggregation is possible in PyRA/TiO<sub>2</sub>.<sup>50</sup>

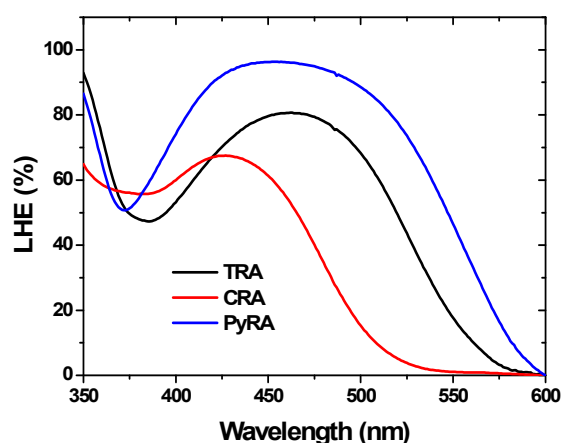


Figure 5: LHE spectra of the TRA, CRA and PyRA adsorbed TiO<sub>2</sub> films.

The light harvesting efficiency (LHE)<sup>51</sup> can be related to the molar extinction coefficient of the dye which is given in the following equation (2),

$$\text{LHE} = 1 - 10^{-\Gamma\sigma(\lambda)} \quad \rightarrow (2)$$

where,  $\Gamma$  (mol cm<sup>-2</sup>) is the number of moles of dye per square centimeter of projected surface area of the film and surface coverage is calculated by using following equation (3),<sup>52-54</sup>

$$\Gamma = A(\lambda)/\sigma(\lambda) \quad \rightarrow (3)$$

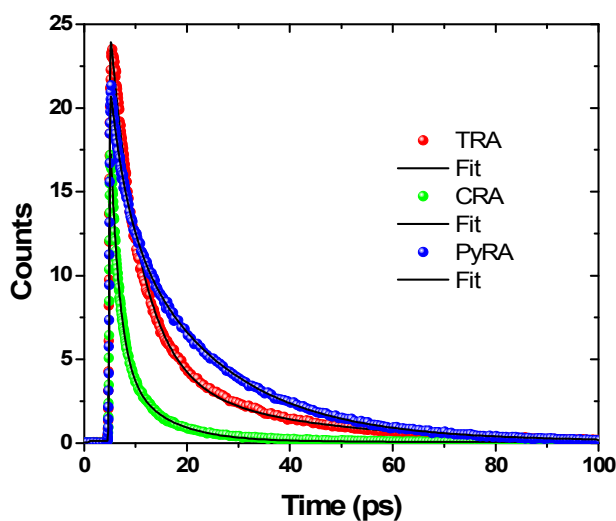
where,  $A(\lambda)$  is the absorbance and  $\sigma(\lambda)$  is the optical cross section at a given wavelength, respectively. Using equation (4), one can able to calculate the  $\sigma(\lambda)$ .

$$\sigma(\lambda) = \varepsilon(\lambda) \times 1000 \text{ (cm}^3 \text{ L}^{-1}) \rightarrow (4)$$

The surface coverage of arylamine dyes were determined to be  $1.46 \times 10^{-8} \text{ mol cm}^{-2}$  for TRA,  $1.43 \times 10^{-8} \text{ mol cm}^{-2}$  for CRA, and  $3.1 \times 10^{-8} \text{ mol cm}^{-2}$  for PyRA. Using these surface coverage values, the LHE spectra of the dye/TiO<sub>2</sub> films are plotted and shown in **figure 5**. From this figure, it is clear that PyRA have higher LHE than others, hence it is expect that PyRA should show higher power conversion efficiency.

### 15 Fluorescence spectroscopy

To get further information about the role of donor moieties on the excited state property of the arylamine dyes, fluorescence spectra were recorded by exciting at their absorption maximum. For fluorescence studies, samples are measured at very dilute solutions in order to avoid the re-absorption, excimer and concentration effect. The fluorescence of arylamine dyes are very weak and they exhibited a very low quantum yields such as 0.0011 (TRA), 0.0006 (CRA) and 0.0019 (PyRA) respectively. A weak fluorescence of arylamine dyes is due to intramolecular charge transfer (ICT). It is previously reported that the ICT is a competitive relaxation process of the singlet excited state and typically reduces the fluorescence.<sup>55</sup> Due to weak fluorescence in nature, it is very difficult to examine the role of donor moiety from the steady state fluorescence studies, hence the time resolved fluorescence measurements has been adopted in order to understand the role of donor moieties. Therefore, femtosecond-fluorescence set up was used to extract the lifetime of the dyes, since the lifetime of these dyes are very fast almost as fast as our TCSPC instrument response function (<50 ps). **Figure 6** display the femtosecond (fs) fluorescence decay of the dyes in methanol were measured in a 100 ps time window upon excitation at 400 nm.



40 **Figure 6:** Time Resolved fluorescence decay of TRA, CRA and PyRA in MeOH

The obtained fluorescence decays are fitted with biexponential function  $[F(t) = A_1 \exp(-t/\tau_1) + A_2 \exp(-t/\tau_2)]$  and the fitted values are collectively given in **table 1**. The ultrafast component of the dyes is at  $\sim 2$  ps, whereas the slow component is slightly longer at  $\sim 20$  ps. The ultrafast decay component,  $\tau_1$  is attributed to the solvent relaxation of the excited states and  $\tau_2$  is due to the lifetime of the relaxed charge transfer state.<sup>56</sup> The obtained average lifetime of the arylamine dyes are in the order of PyRA>TRA>CRA. However, the obtained lifetimes are in the picosecond time scales, hence the electron injection from these dyes to TiO<sub>2</sub> is expected to be very fast.<sup>56-58</sup>

**Table 1:** Fitting parameters of arylamine derivatives in THF

Dyes	$\lambda_{\text{emi}}^a$	$\tau_1$ (ps)	$\tau_2$ (ps)	$A_1$ (%)	$A_2$ (%)	$\tau_{\text{av}}$ (ps)
TRA	590	5.8	29.7	83	17	9.8
CRA	540	1.7	8.3	74	26	3.41
PyRA	550	3.2	19.1	35	65	13.53

<sup>a</sup> Probing wavelength (nm)

### Solvatochromism

It is well known that, excited state properties of the ICT based dyes were found to be very sensitive to the solvent polarity.<sup>59</sup> Hence, solvatochromism of arylamine dyes were performed. The solvatochromic method is based on the shift of the UV-Vis absorption and fluorescence maxima with varying polarity of the solvent.<sup>60</sup> The absorption and fluorescence spectra of dyes with varying solvents are shown in **figure S10-S15** and the corresponding maxima are listed in **table S1**. All the dyes show a structured emission in nonpolar solvents, whereas moderate and high polarity solvents show a broad and structureless emission. Stokes' shift is calculated as the difference between absorption and emission maxima obtained from the corrected spectra on the wavenumber scale. The obtained large Stokes' shift is a result of efficient charge transfer from the arylamine donor moiety to the acceptor rhodanine-3-acetic acid moiety (*cf. above*). Moreover, all the dyes were found to be completely insoluble in water and hence the photophysical parameters could not be obtained in water ( $\varepsilon=80$ ).

Solvent dependent spectral shifts are often interpreted in terms of the Lippert equation (5), which describes Stokes' shift in terms of the change in dipole moment of the fluorophore upon excitation and the dependence of energy of the dipole on the dielectric constant and refractive index of the solvent<sup>61</sup> and is given as:

$$\bar{\nu}_A - \bar{\nu}_F = \frac{2}{hc} \left( \frac{\varepsilon - 1}{2\varepsilon + 1} - \frac{n^2 - 1}{2n^2 + 1} \right) \frac{(\mu_E - \mu_G)^2}{a^3} + \text{constant} \rightarrow (5)$$

Where,  $\bar{\nu}_A$  and  $\bar{\nu}_F$  are the wavenumbers ( $\text{cm}^{-1}$ ) of the absorption and emission,  $h$  is Planck's constant,  $c$  is the speed of light,  $a$  is the radius of the cavity,  $\varepsilon$  is the dielectric constant of

the medium,  $n$  is the refractive index of the solvent and the term  $\Delta f$  is the orientation polarizability (eq. 6).

$$\Delta f = \frac{\epsilon - 1}{2\epsilon + 1} - \frac{n^2 - 1}{2n^2 + 1} \rightarrow (6)$$

**Figure 7** represents the Lippert–Mataga plot of arylamine dyes in various solvents. Alcoholic solvents were omitted in order to get a linear correlation. Since, these solvents are involved in specific solute-solvent interactions.<sup>62</sup>

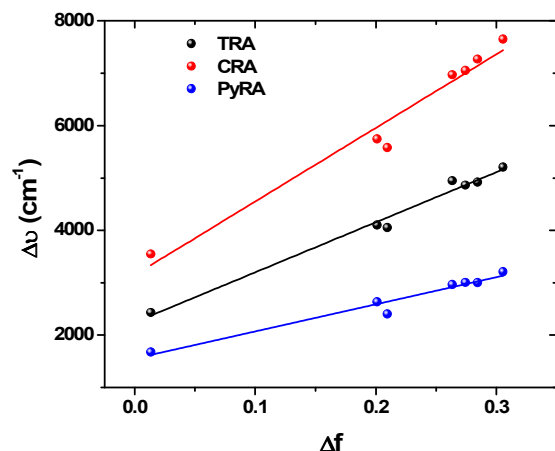


**Figure 7:** Lippert–Mataga plots for the dyes.

A specific solvent interaction is further verified by varying percentage of alcohol into a non-polar solvent. For instance, the emission spectrum of TRA in pure toluene is structured, whereas in methanol it is weak, broad and structureless (**Figure 8**). In the binary mixture as the methanol amount increases, there is a loss in vibrational fine structure of the TRA spectrum and also a decrease in the overall spectral intensity is observed. Moreover, increase in methanol there is a gradual red-shift in the emission maximum. The most likely explanation for the above observed spectral changes could be the preferential solvation of the polar excited ICT state by a more polar solvent. In toluene, due to the absence of a solvent dipole, the emission is from the locally excited state showing a structured spectrum.

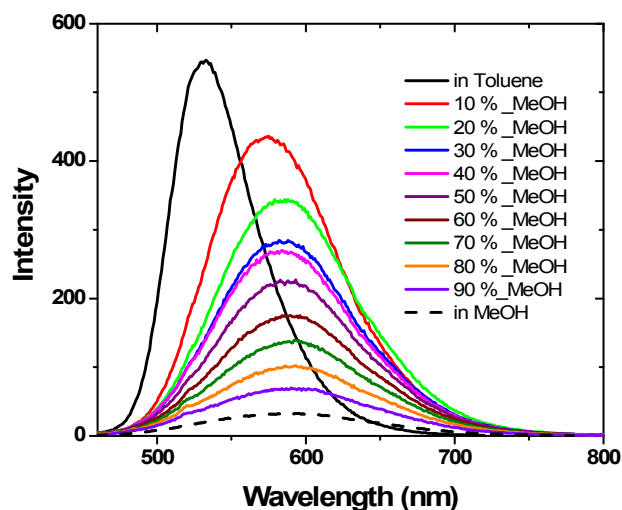


**Figure 8:** Fluorescence spectra of TRA in toluene–methanol mixtures.

**Figure 7** shows the linear plot of solvent polarity function versus Stokes' shift. The change in dipole moment ( $\Delta\mu = \mu_e - \mu_g$ ) for all the dyes have been calculated from the slope of the linear plot and are listed in **table 2**. The estimated  $\Delta\mu$  values are more positive (**Table 2**) and suggestive of a large dipole moment for the molecules in the excited state. Among the dyes, TRA and CRA exhibit a large change in dipole moment confirming the more pronounced ICT for these molecules in the excited state. The emission spectra of dyes are broadened on moving from nonpolar to the polar solvents. This probably supports the speculation that the initially formed local excited state transforms into the more polar charge transfer state, which is stabilized by the polar solvents. Thus significant change in dipole moment on excitation has been observed.

**Table 2:** Ground and excited state dipole moment of the dyes

Dyes	Radius (Å)	$\mu_G$ (D) <sup>a</sup>	$\Delta\mu$ (D) <sup>b</sup>	$\mu_E$ (D) <sup>c</sup>
TRA	6.17	11.08	14.9	25.98
CRA	6.02	4.53	17.4	21.93
PyRA	5.61	8.55	9.52	18.07

<sup>a</sup> Estimated from the B3LYP/6-311+G\*\* calculations

<sup>b</sup> calculated from the slope of the linear L-M plot

<sup>c</sup>  $\mu_E = \Delta\mu + \mu_G$

### Electrochemical properties

Electrochemical properties of arylamine dyes were investigated by cyclic voltammetry (CV) and differential pulse voltammetry (DPV) in deoxygenated ACN solution containing 0.1 M tetra-n-butylammonium hexafluorophosphate (TBAPF<sub>6</sub>) as supporting electrolyte (**Figure S16**). The measurements were carried out using a typical three-electrode electrochemical cell, which consists of glassy carbon electrode which is used as the working electrode while platinum wire and Ag/AgCl were used as the counter and reference electrodes, respectively. All of the dyes show an oxidation wave which is attributable to the removal of an electron from the amine segment. The exact oxidation potential for the arylamine dyes was extracted from the DPV method and listed in **table 3**. As shown in this **table**, the first oxidation potentials ( $E_{ox}$ ) correspond to the HOMO levels of the dyes, which are more positive than the redox potential of the (I/I<sub>3</sub>)<sup>-</sup> redox couple (0.4 V), indicating that reduction of the oxidized dyes with I<sup>-</sup> ions is thermodynamically feasible. On the other hand, the excited state oxidation potentials ( $E_{ox}^*$ ), which correspond to the LUMO level of the dyes and this can be obtained by the following equation (7):

$$E_{ox}^* = E_{ox} - E_{(0-0)} \rightarrow (7)$$

where,  $E_{(0-0)}$  is the excited state energy of the dye, which is estimated from the intersection between the normalized absorption and emission spectra. The obtained  $E_{ox}^*$  of the dyes are more negative than the conduction band potential of TiO<sub>2</sub> (-0.5 V vs NHE), indicating that the electron injection process from the excited dyes to the TiO<sub>2</sub> conduction band is energetically favourable (**Scheme 1**).

Driving forces for electron injection ( $\Delta G_{inj}$ ) from the dye excited state to the CB of  $\text{TiO}_2$  and electron recombination ( $\Delta G_{rec}$ ) from the CB of  $\text{TiO}_2$  to the dye radical cation ( $E_{ox}$ ) are determined from the following equations and values are shown in **table 3**.

$$\Delta G_{inj} = E_{ox}^* - E_{CB} \quad \rightarrow (8)$$

$$\Delta G_{rec} = E_{CB} - E_{ox} \quad \rightarrow (9)$$

The obtained  $\Delta G$  values are negative, which indicated that both of the processes are thermodynamically feasible and most importantly injection is dominant process than recombination for these dyes.

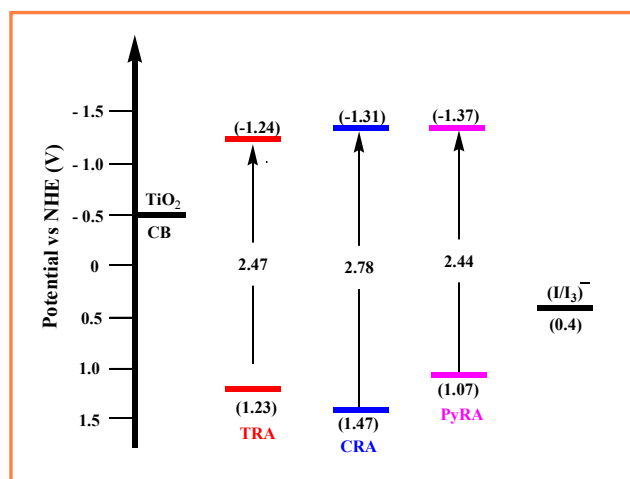
**Table 3:** Electrochemical Data and Driving Forces for Electron Transfer Processes on  $\text{TiO}_2$

Dyes	<sup>a</sup> $E_{0-0}/\text{eV}$	$E_p/\text{V}$	<sup>b</sup> $E_{ox}/\text{eV}$	<sup>c</sup> $E_{ox}^*/\text{eV}$	$\Delta G_{inj}$	$\Delta G_{rec}$
TRA	2.47	1.03	1.23	-1.24	-0.74	-1.73
CRA	2.78	1.27	1.47	-1.31	-0.81	-1.97
PyRA	2.44	0.87	1.07	-1.37	-0.87	-1.57

<sup>a</sup>  $E_{0-0}$  values were calculated from intersect of the normalized absorption and the emission spectra

<sup>b</sup>  $E_{ox}$  was measured in acetonitrile with 0.1 M TBAPF<sub>6</sub> as supporting electrolyte. Potentials measured vs Ag/AgCl were converted to normal hydrogen electrode (NHE) by addition of + 0.2 V.  $E_p$  is the peak potential of DPV,  $E_{ox} = E_p + 0.2$  V.

<sup>c</sup> The excited state oxidation potential (vs NHE), calculated from  $E_{ox} - E_{0-0}$ .



**Scheme 1:** Schematic energy levels for the electron transfer between arylamine dyes and conduction band of  $\text{TiO}_2$ .

### Photovoltaic properties

Overall results clearly enlightens that the dyes developed in this work have a promising light absorption properties and suitable ground/excited state oxidation potentials to use them as potential sensitizers for conventional DSCs. In addition, the results from DFT calculations, photophysical and electrochemical studies reveal that PyRA may have potential candidate for solar cells. Hence, the photovoltaic studies of the freshly fabricated cells are measured under AM1.5 solar irradiation ( $85 \text{ mW}/\text{cm}^2$ ) and the corresponding J-V characteristic of the cells are shown in **figure 9**.

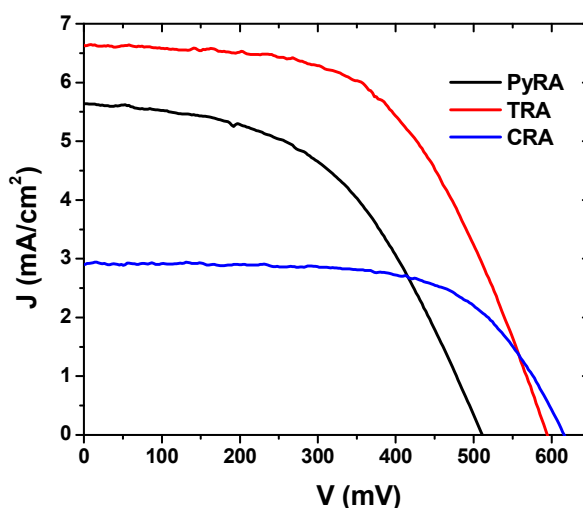


**Figure 9:** J-V characteristics of the TRA, CRA and PyRA devices.

The parameters such as short-circuit current density ( $J_{SC}$ ), open-circuit voltage ( $V_{OC}$ ), fill factor (FF) and overall conversion efficiency ( $\eta$ ) were summarized in **table 4**. From the results, it is clear that there is a significant role of donor moieties on the power conversion efficiency. For instance, taking TRA as a prototype, PyRA and CRA molecules were developed in order to understand the impact of donor moiety on the performance of the solar cells. There are several groups reported the power conversion efficiency of TRA<sup>63-65</sup> around 2.5%, here we have also reproduced the same, hence it is meaningful to compare the newly developed molecules (PyRA and CRA). Under same condition, the PyRA and CRA sensitized solar cells consequences the overall power conversion efficiencies ( $\eta$ ) of 1.68 % and 1.25 % respectively. It is clear that the photovoltaic performances of DSCs are affected by changing the electron rich donors in organic dyes. By comparing PyRA and CRA, the photovoltaic performance of PyRA is significantly improved; this may due to the higher molar extinction coefficient and high  $J_{SC}$ . Contrary to our expectation, the power conversion efficiency of PyRA is less than TRA. In order to examine why such a difference in power conversion efficiency occurred, the electrochemical impedance spectroscopy<sup>66</sup> was employed. **Figure 10** shows the EIS Nyquist plots for DSCs based on TRA, CRA and PyRA. Generally, the largest semicircle in the lower frequency range in the Nyquist plot represents the interfacial charge transfer at the  $\text{TiO}_2/\text{dye}/\text{electrolyte}$  interface,<sup>67</sup> which is the charge recombination between injected electrons and electrolyte.

**Table 4:** Photovoltaic properties of TRA, CRA and PyRA devices.

Dyes	$J_{SC}/\text{mA cm}^{-2}$	$V_{OC}/\text{V}$	FF	$\eta(\%)$	$\tau(\text{ms})$
TRA	6.63	0.59	0.55	2.57	17.58
CRA	2.92	0.61	0.59	1.25	13.26
PyRA	5.65	0.51	0.49	1.68	4.29

Hence, the obtained plot in **figure 10** looks like a semicircle which is assigned to the charge transfer resistance at the TiO<sub>2</sub>/dye/electrolyte interface. The diameter of the semicircle is in the order of: TRA>CRA>PyRA, which means that the electron transfer resistance for the unwanted back reaction is larger for TRA than that of CRA and PyRA. This may be responsible for the achieved higher V<sub>OC</sub> and J<sub>SC</sub> of TRA. Moreover, the electron recombination between the electrolyte and TiO<sub>2</sub> and is related to the electron lifetime in the CB of TiO<sub>2</sub>, which is ultimately related to V<sub>OC</sub>. Therefore, Bode phase plots (**Figure S17**) were used to find out the effective lifetime ( $\tau_{\text{eff}}$ ) of electrons in the conduction band of TiO<sub>2</sub>.  $\tau_{\text{eff}}$  were calculated<sup>68</sup> by making use of the following equation (10)

$$\tau_{\text{eff}} = 1/2\pi f \rightarrow (10)$$

where, f is the frequency of the corresponding peak in the Bode phase plot. The obtained electron lifetimes for TRA, CRA and PyRA are 17.58, 13.26 and 4.29 ms, respectively. In principle, a longer electron lifetime indicate improved suppression of back reactions between the injected electrons and the electrolyte that lead to improvement of the V<sub>OC</sub> value, due to the reduced electron recombination rate.<sup>69</sup> Consequently, the observed longer electron lifetime in case of TRA could explain its high V<sub>OC</sub> and also the higher efficiency as well as more effective suppression of back reaction than other dyes (PyRA and CRA).

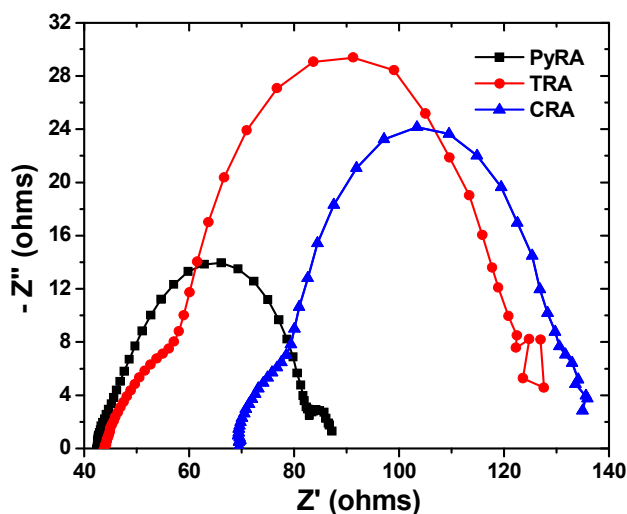


**Figure 10:** Nyquist plots of TRA, CRA and PyRA devices.

### Summary

We have successfully demonstrated the impact of donor moiety on the photophysical and photovoltaic properties of certain arylamine derivatives. Among the dyes investigated TRA and PyRA shows strong absorption characteristics due to reduced HOMO/LUMO energy gaps than CRA. The excited state lifetime of these dyes are almost similar (in the order of picoseconds time scale) and the electron injection is expected to be same, as a result one can expect similar power conversion efficiency. In contrary to the expectation, power conversion efficiency of TRA (2.57%) and PyRA (1.68%) is very diverse. The higher power

conversion efficiency of TRA is due to high J<sub>SC</sub> and V<sub>OC</sub> values. The lower power conversion efficiency of PyRA is due to faster electron recombination rate as evidenced by electrochemical impedance spectroscopy. These findings reveal that diminutive alteration in the structure of donor moiety play a significant role in photovoltaic performance.

### Acknowledgment

A.K. thanks DST, India for the DST-SERB Project (Ref. No. CS-316/2012, Dt. 04/12/2012) and M.J. thanks to DST, India for DST-INSPIRE Faculty Award [IFA13-CH-100].

### Notes

- <sup>1</sup> National Centre for Ultrafast Processes, University of Madras, Taramani Campus, Chennai – 600 113, Tamil Nadu, India
- <sup>2</sup> Department of Chemistry, Loyola College, Chennai – 600 034, Tamil Nadu, India
- <sup>3</sup> Nanomaterials and Solar Energy Conversion Laboratory, Department of Chemistry, National Institute of Technology, Tiruchirappalli - 620 015, Tamil Nadu, India

\* Author for correspondence  
E-mail address: [akathir23@hotmail.com](mailto:akathir23@hotmail.com) (Dr. A. Kathiravan)

<sup>65</sup> Electronic Supplementary Information (ESI) available.

### References

- <sup>1</sup> B. O'Regan, and M. Grätzel, *Nature*, 1991, 353, 737–740.
- <sup>2</sup> A. Hagfeldt, G. Boschloo, L. Sun, L. Kloo, and H. Pettersson, *Chem. Rev.*, 2010, 110, 6595–663.
- <sup>3</sup> L.L. Li, and E. W. G. Diau, *Chem. Soc. Rev.*, 2013, 42, 291–304.
- <sup>4</sup> W. M. Campbell, A. K. Burrell, D. L. Officer, and K. W. Jolley, *Coord. Chem. Rev.*, 2004, 248, 1363–1379.
- <sup>5</sup> A. Kira, Y. Matsubara, H. Iijima, T. Umeyama, Y. Matano, S. Ito, M. Niemi, N. V. Tkachenko, H. Lemmetyinen, and H. Imahori, *J. Phys. Chem. C*, 2010, 114, 11293–11304.
- <sup>6</sup> M.V. Martinez-Diaz, G. de la Torrea, and T. Torres, *Chem. Commun.* 2010, 46, 7090–7108.
- <sup>7</sup> L. Han, A. Islam, H. Chen, C. Malapaka, B. Chiranjeevi, S. Zhang, X. Yang, and M. Yanagida, *Energy Environ. Sci.*, 2012, 5, 6057–6060.
- <sup>8</sup> M.K. Nazeeruddin, F. De Angelis, S. Fantacci, A. Selloni, G. Viscardi, P. Liska, S. Ito, B. Takeru, and M. Grätzel, *J. Am. Chem. Soc.*, 2005, 127, 16835–16847.
- <sup>9</sup> F. Gao, Y. Wang, D. Shi, J. Zhang, M. Wang, X. Jing, R. Humphry-Baker, P. Wang, S.M. Zakeeruddin, and M. Grätzel, *J. Am. Chem. Soc.*, 2008, 130, 10720–10728.
- <sup>10</sup> T. Bessho, S. M. Zakeeruddin, C-Y. Yeh, E. W-G. Diau, and M. Grätzel, *Angew. Chem., Int. Ed.* 2010, 49, 6646–6649.
- <sup>11</sup> S.L. Wu, H.P. Lu, H.T. Yu, S.H. Chuang, C.L. Chiu, C.W. Lee, E. W.G. Diau, and C. Y. Yeh, *Energy Environ. Sci.*, 2010, 3, 949–955.
- <sup>12</sup> H. Imahori, Y. Matsubara, H. Iijima, T. Umeyama, Y. Matano, S. Ito, M. Niemi, N. V. Tkachenko, and H. Lemmetyinen, *J. Phys. Chem. C*, 2010, 114, 10656–10665.

- 13 S. Eu, S. Hayashi, T. Umeyama, A. Oguro, M. Kawasaki, N. Kadota, Y. Matano, and H. Imahori, *J. Phys. Chem. C*, 2007, 111, 3528–3537.
- 5 14 C.L. Wang, Y.C. Chang, C.M. Lan, C.F. Lo, E.W.G. Diau, and C.Y. Lin, *Energy Environ. Sci.*, 2011, 4, 1788–1795.
- 15 15 C.M. Lan, H.P. Wu, T.Y. Pan, C.W. Chang, W.S. Chao, C.T. Chen, C.L. Wang, C.Y. Lin, and E.W.G. Diau, *Energy Environ. Sci.*, 2012, 5, 6460–6464.
- 10 16 K. Kurotobi, Y. Toude, K. Kawamoto, Y. Fujimori, S. Ito, P. Chabera, V. Sundström, and H. Imahori, *Chem. Eur. J.*, 2013, 19, 17075–17081.
- 15 17 H. Imahori, T. Umeyama, and S. Ito, *Acc. Chem. Res.*, 2009, 42, 1809–1818.
- 18 18 T. Higashino, and H. Imahori, *Dalton Trans.*, 2015, 44, 448–463.
- 20 19 Y. Liu, N. Xiang, X. Feng, P. Shen, W. Zhou, C. Weng, B. Zhao, and S. Tan, *Chem. Commun.*, 2009, 2499–2501.
- 25 20 M.K. Panda, G.D. Sharma, K.R.J. Thomas, and A.G.A. Coutsolelos, *J. Mater. Chem.*, 2012, 22, 8092–8102.
- 30 21 W.M. Campbell, K.W. Jolley, P. Wagner, K. Wagner, P.J. Walsh, K. C. Gordon, L. Schmidt-Mende, M.K. Nazeeruddin, Q. Wang, M. Grätzel, and D.L. Officer, *J. Phys. Chem. C*, 2007, 111, 11760–11762.
- 35 22 M.K. Nazeeruddin, R. Humphry-Baker, D.L. Officer, W.M. Campbell, A.K. Burrell, and M. Grätzel, *M. Langmuir*, 2004, 20, 6514–6517.
- 40 23 A. Yella, C.L. Mai, S.M. Zakeeruddin, S.N. Chang, C.H. Hsieh, C.Y. Yeh, and M. Grätzel, *Angew. Chem., Int. Ed.*, 2014, 53, 2973–2977.
- 45 24 S. Mathew, A. Yella, P. Gao, R. Humphry-Baker, F.E. Curchod Basile, N. Ashari-Astani, I. Tavernelli, U. Rothlisberger, K.M. Nazeeruddin, and M. Grätzel, *Nat. Chem.*, 2014, 6, 242–247.
- 50 25 A. Mishra, M.K.R. Fischer and P. Bauerle, *Angew. Chem., Int. Ed.*, 2009, 48, 2474–2499.
- 55 26 A. Hagfeldt, G. Boschloo, L. Sun, L. Kloo, and H. Pettersson, *Chem. Rev.*, 2010, 110, 6595–6663.
- 60 27 W.D. Zeng, Y.M. Cao, Y. Bai, Y.H. Wang, Y.S. Shi, M. Zhang, F.F. Wang, C. Pan, and P. Wang, *Chem. Mater.*, 2010, 22, 1915–1925.
- 65 28 H.N. Tsao, J. Burschka, C. Yi, F. Kessler, M.K. Nazeeruddin, and M. Grätzel, *Energy Environ. Sci.*, 2011, 4, 4921–4924.
- 70 29 M. Zhang, Y. Wang, M. Xu, W. Ma, R. Li and P. Wang, *Energy Environ. Sci.*, 2013, 6, 2944–2949.
- 75 30 M. Liang, W. Xu, F.S. Cai, P.Q. Chen, B. Peng, J. Chen, and Z.M. Li, *J. Phys. Chem. C*, 2007, 111, 4465.
- 80 31 P. Daniel, J.H. Yum, H.J. Lee, F.D. Angelis, T. Marinado, K. M. Karlsson, R.H. Baker, L. Sun, A. Hagfeldt, M. Grätzel, and M.K. Nazeeruddin, *J. Am. Chem. Soc.*, 2008, 130, 6259–6266.
- 85 32 M. Frisch et al. Gaussian 09, Revision D. 01, Gaussian, Inc., Wallingford, CT, 2010.
- 90 33 A.D. Becke, *J. Chem. Phys.*, 1993, 98, 5648–5652.
- 95 34 C. Lee, W. Yang and R.G. Parr, *Phys. Rev. B: Condens. Matter Mater. Phys.*, 1988, 37, 785–789.
- 100 35 J.P. Perdew, *Phys. Rev. B: Condens. Matter Mater. Phys.*, 1986, 33, 8822–8824.
- 105 36 A. Kathiravan, K. Sundaravel, M. Jaccob, G. Dhinakaran, A. Rameshkumar, D. Arul Ananth, and T. Sivasudha, *J. Phys. Chem. B*, 2014, 118, 13573–13581.
- 110 37 D.V. Talapin, R. Koeppel, S. Goetzinger, A. Kornowski, J.M. Lupton, A.L. Rogach, O. Benson, J. Feldmann, and H. Weller, *Nano Lett.*, 2003, 3, 1677–1681.
- 115 38 J. Shen, and R.D. Snook, *Chem. Phys. Lett.*, 1989, 155, 583–586.
- 120 39 N. Pavithra, A. Asiri, and S. Anandan, *J. Power Sources*, 2015, 286, 346–353.
- 125 40 J. Feng, Y. Jiao, W. Ma, M.K. Nazeeruddin, M. Grätzel and S. Meng, *J. Phys. Chem. C*, 2013, 117, 3772–3778.
- 130 41 A. Dualeh, F. De Angelis, S. Fantacci, T. Moehl, C. Yi, F. Kessler, E. Baranoff, M.K. Nazeeruddin and M. Grätzel, *J. Phys. Chem. C*, 2012, 116, 1572–1578.
- 135 42 C.H. Yang, S.H. Liao, Y.K. Sun, Y.Y. Chuang, T.L. Wang, Y.T. Shieh, and W.C. Lin, *J. Phys. Chem. C*, 2010, 114, 21786–21794.
- 140 43 D. Kuang, S. Ito, B. Wenger, C. Klein, J.E. Moser, R.H. Baker, S.M. Zakeeruddin, and M. Grätzel, *J. Am. Chem. Soc.*, 2006, 128, 4146–4154.
- 145 44 M.K. Nazeeruddin, S.M. Zakeeruddin, R. Humphry-Baker, M. Jirousek, P. Liska, N. Vlachopoulos, V. Shklover, C.H. Fischer, and M. Grätzel, *Inorg. Chem.*, 1999, 38, 6298–6305.
- 150 45 D. Zhang, V. Martin, I.G. Moreno, A. Costela, M.E.P. Ojeda, and Y. Xiao, *Phys. Chem. Chem. Phys.*, 2011, 13, 13026–13033.
- 155 46 J.A. Mikroyannidis, A. Kabanakis, P. Balraju, and G.D. Sharma, *J. Phys. Chem. C*, 2010, 114, 12355–12363.
- 160 47 L.L. Tan, H.Y. Chen, L.F. Hao, Y. Shen, L.M. Xiao, J.M. Liu, D.B. Kuang and C.Y. Su, *Phys. Chem. Chem. Phys.*, 2013, 15, 11909–11917.
- 165 48 D.P. Hagberg, J.H. Yum, H. Lee, F. DeAngelis, T. Marinado, and K. Karlsson, *J. Am. Chem. Soc.*, 2008, 130, 6259–6266.
- 170 49 F. Nüesch, J.E. Moser, V. Shklover, and M. Grätzel, *J. Am. Chem. Soc.*, 1996, 118, 5420–5431.
- 175 50 C.Y. Lee, C. She, N.C. Jeong, and J.T. Hupp, *Chem. Commun.*, 2010, 46, 6090–6092.
- 180 51 M.K. Nazeeruddin, A. Kay, L. Rodicio, R. Humphry-Baker, E. Müller, P. Liska, N. Vlachopoulos, and M. Grätzel, *J. Am. Chem. Soc.*, 1993, 115, 6382–6390.
- 185 52 H. C. Zhao, J.P. Harney, Y.T. Huang, J.H. Yum, M.K. Nazeeruddin, M. Grätzel, M.K. Tsai, and J. Rochford, *Inorg. Chem.*, 2012, 51, 1–3.
- 190 53 S.A. Trammell, and T.J. Meyer, *Langmuir*, 2003, 19, 6081–6087.
- 195 54 P.G. Hoertz, Z.F. Chen, C.A. Kent, and T.J. Meyer, *Inorg. Chem.*, 2010, 49, 8179–8181.
- 200 55 A. Cidlina, V. Novakova, M. Miletina, P. Zimcik, *Dalton Trans.*, 2015, 44, 6961–6971.
- 205 56 M. Ziolek, I. Tacchini, M.T. Martinez, X. Yang, L. Sun and A. Douhal, *Phys. Chem. Chem. Phys.*, 2011, 13, 4032–4044.

- 57 J.M. Rehm, G.L. McLendon, Y. Nagasawa, Y. Nagasawa, J. Moser and M. Grätzel, *J. Phys. Chem.*, 1996, 100, 9577-9578.
- 58 O. Bram, A. Cannizzo and M. Chergui, *Phys. Chem. Chem. Phys.*, 2012, 14, 7934–7937.
- 59 H. Li, Y. Guo, Y. Lei, W. Gao, M. Liu, J. Chen, Y. Hu, X. Huang, H. Wu, *Dyes pigm.*, 2015, 112, 105-115.
- 60 A. Marini, A.M. Losa, A. Biancardi, and B. Mennucci, *J. Phys. Chem. B*, 2010, 114, 17128–17135.
- 61 J.R. Lakowicz, Springer Publishers, New York, 2006.
- 62 I. Bylinska, M. Wierzbicka, C. Czaplewski and W. Wicz, *RSC Adv.*, 2014, 4, 48783–48795.
- 63 T. Marinado, D.P. Hagberg, M. Hedlund, T. Edvinsson, E.M.J. Johansson, G. Boschloo, H. Rensmo, T. Brinck, L. Sun and A. Hagfeldt, *Phys. Chem. Chem. Phys.*, 2009, 11, 133–141.
- 64 C.H. Yang, W.C. Lin, T.L. Wang, Y.T. Shieh, W.J. Chen, S.H. Liao, and Y.K. Sun, *Mater. Chem. Phys.*, 2011, 130, 635– 643.
- 65 C.A. Echeverry, A. Insuasty, M.A. Herranz, A. Ortíz, R. Cotta, V. Dhas, L. Echevoyen, B. Insuasty, and N. Martín, *Dyes Pigm.*, 2014, 107, 9-14.
- 66 Q. Wang, J.E. Moser and M. Grätzel, *J. Phys. Chem. B*, 2005, 109, 14945-14953.
- 67 N. Koide, A. Islam, Y. Chiba and L.Y.J. Han, *J. Photochem. Photobiol. A: Chem.*, 2006, 182, 296-305.
- 68 D.D. Babu, S.R. Gachumale, S. Anandan and A.V. Adhikari, *Dyes Pigm.*, 2015, 112, 183-191.
- 69 D. Kuang, S. Uchida, R. Humphry-Baker, S.M. Zakeeruddin and M. Grätzel, *Angew. Chem., Int. Ed.*, 2008, 47, 1923-1927.